

1 **The Effect of the 2013-2016 High Temperature Anomaly in the Subarctic Northeast Pacific**  
2 **(The “Blob”) on Net Community Production**

3 Bo Yang<sup>1†</sup>, Steven R. Emerson<sup>1</sup>, M. Angelica Peña<sup>2</sup>

4 <sup>1</sup> School of Oceanography, University of Washington, Seattle, WA 98195, USA

5 <sup>2</sup> Institute of Ocean Sciences, Fisheries and Oceans Canada, PO Box 6000, Sidney, BC, Canada,  
6 V8L 4B2

7 <sup>†</sup>Present Address: Department of Environmental Sciences, University of Virginia, Charlottesville,  
8 VA 22904

9 Corresponding author: Bo Yang (by3jr@virginia.edu)

10 Email address: Steven R. Emerson (emerson@uw.edu), M. Angelica Peña (Angelica.Pena@dfo-  
11 mpo.gc.ca)

12 Key words: The warm blob, net community production, ocean station Papa

13

## 14 **Abstract**

15           A large anomalously warm water patch (the “Blob”) appeared in the NE Pacific Ocean in  
16 the winter of 2013–14 and persisted through 2016 causing strong positive upper ocean  
17 temperature anomalies at Ocean Station Papa (OSP, 50°N, 145°W). The effect of the  
18 temperature anomalies on annual net community production (ANCP) was determined by upper  
19 ocean chemical mass balances of O<sub>2</sub> and DIC using data from a profiling float and a surface  
20 mooring. Year-round oxygen mass balance in the upper ocean (0 to 91–111 m) indicates that  
21 ANCP decreased after the first year when warmer water invaded this area and then returned to  
22 the “pre-blob” value (2.4, 0.8, 2.1, and 1.6 mol C m<sup>-2</sup> yr<sup>-1</sup> from 2012 to 2016, with a mean value  
23 of 1.7 ± 0.7 mol C m<sup>-2</sup> yr<sup>-1</sup>). ANCP determined from DIC mass balance has a mean value that is  
24 similar within the errors as that from the O<sub>2</sub> mass balance but without significant trend (2.0, 2.1,  
25 2.6, and 3.0 mol C m<sup>-2</sup> yr<sup>-1</sup> with a mean value of 2.4 ± 0.6 mol C m<sup>-2</sup> yr<sup>-1</sup>). This is likely due to  
26 differences in the air-sea gas exchange, which is a major term for both mass balances. Oxygen  
27 has a residence time with respect to gas exchange of about one month while the CO<sub>2</sub> gas  
28 exchange response time is more like a year. Therefore the biologically induced oxygen saturation  
29 anomaly responds fast enough to record annual changes whereas that for CO<sub>2</sub> does not.  
30 Phytoplankton pigment analysis from the upper ocean shows lower chlorophyll-*a* concentrations  
31 and greater relative abundance of picoplankton in the year after the warm water patch entered the  
32 area than in previous and subsequent years. Our analysis of multiple physical and biological  
33 processes that may have caused the ANCP decrease after warm water entered the area suggests  
34 that it was most likely due to changes in plankton community composition.

## 35 **1 Introduction**

36 Net community production (NCP) in the upper ocean is defined as net organic carbon  
37 production, which equals biological production minus respiration. At steady state when  
38 integrated over a period of at least one year, the annual NCP (ANCP) is equivalent to the flux of  
39 biologically-produced organic matter from the upper ocean to the interior. Both biological  
40 production and respiration processes are temperature dependent, and heterotrophic activities such  
41 as community respiration and zooplankton grazing are usually considered to be more sensitive to  
42 temperature change than autotrophic production (Allen et al., 2005; Brown et al., 2004; Gillooly  
43 et al., 2001; López-Urrutia et al., 2006; Regaudie-De-Gioux and Duarte, 2012; Rose and Caron,  
44 2007). This implies that rising temperature should lead to enhanced heterotrophy and lower NCP  
45 (López-Urrutia et al., 2006). In contrast, it has also been suggested (e.g., Chen and Laws, 2017)  
46 that the main effect of temperature on community metabolism is likely due to differences in  
47 phytoplankton community composition (e.g. cyanobacteria dominate in warm, oligotrophic  
48 waters, whereas diatoms dominate in cold, nutrient-rich areas) rather than to lower temperature  
49 sensitivity of phytoplankton production.

50 From the winter of 2013, a large anomalously warm water patch (the “Blob”) appeared  
51 in the NE Pacific Ocean (Bond et al., 2015). The “Blob” had stretched from Alaska to Baja  
52 California by the end of 2015 (Di Lorenzo and Mantua, 2016) and caused widespread changes in  
53 the marine ecosystem, such as geographical shifts of plankton species, harmful algal blooms, and  
54 strandings of fishes, marine mammals, and seabirds (Cavole et al., 2016). Here we calculate the  
55 ANCP with upper ocean oxygen (O<sub>2</sub>) and dissolved inorganic carbon (DIC) mass balances using  
56 data from Ocean Station Papa in the NE Pacific (OSP, 50°N, 145°W, Figure 1), to determine if  
57 there were significant NCP changes during the anomalous warm event. The monthly Sea Surface

58 Temperature Anomaly (SSTA) at OSP from 2012 to 2016 (Figure 2) indicates that for most of  
59 the 1<sup>st</sup> year (starting from June 2012) sea surface temperature (SST) was lower than usual, but  
60 then transitioned to strong positive temperature anomaly from 2013 to 2014. The positive  
61 anomaly continued with a magnitude of ~ 2°C to June 2015, and then dropped back to “normal”  
62 in the summer of 2016.

63 Our field location is in the subarctic northeast Pacific Ocean at OSP, where repeat  
64 hydrographic cruises have been carried out since 1981 by Fisheries and Oceans Canada with a  
65 frequency of two to three times per year (Freeland, 2007). A NOAA surface mooring has been  
66 deployed at OSP since 2007, for physical and biogeochemical measurements such as  
67 temperature, salinity, wind, ocean current, radiation, oxygen and total gas pressure, pH, and  
68 carbon dioxide (CO<sub>2</sub>) (Emerson et al. 2011; Cronin et al. 2015; Fassbender et al. 2016). In  
69 addition, Argo profiling floats have been deployed near OSP since the 2000s (Freeland and  
70 Cummins, 2005). The first floats measured only temperature, salinity, and pressure but then  
71 measurements of oxygen and nitrate were added (Bushinsky and Emerson, 2015; Johnson et al.,  
72 2009). NCP at OSP has been determined using various approaches over the years, including  
73 bottle incubations (Wong, 1995), <sup>234</sup>Th methods (Charette et al., 1999), carbon/nutrient  
74 drawdown (Fassbender et al., 2016; Plant et al., 2016; Takahashi et al., 1993; Wong et al., 2002a,  
75 2002b), and oxygen mass balance (Bushinsky and Emerson, 2015; Emerson, 1987; Emerson et  
76 al., 1991, 1993; Giesbrecht et al., 2012; Juranek et al., 2012; Plant et al., 2016).

## 77 **2 Methods**

### 78 **2.1 Measurements of O<sub>2</sub>, DIC, and phytoplankton biomass**

79 Autonomous in situ oxygen measurements were made on a profiling float deployed by  
80 the University of Washington (Special Oxygen Sensor Argo float, SOS-Argo F8397, WMO #

81 5903743, Figure 1). The complete dataset is available at  
82 <https://sites.google.com/a/uw.edu/sosargo/>, and some of the data have been published previously  
83 by Bushinsky and Emerson (2015) and Yang et al. (2017). Oxygen measurements on the SOS-  
84 Argo float were obtained using an Aanderaa optode oxygen sensor with air-calibration  
85 mechanism (Bushinsky et al., 2016) capable of providing the air-sea difference in oxygen  
86 concentration with an accuracy of about  $\pm 0.2\%$  and a vertical resolution of 3-5 m in the top 200  
87 m of water column. This float was operated at a cycle interval of  $\sim 5$  days covering depths from  
88 surface to 1800 m.

89 Partial pressure of seawater CO<sub>2</sub> ( $p\text{CO}_2$ ), temperature, and salinity data were obtained  
90 from the NOAA mooring at OSP (WMO # 4800400). The complete dataset is available at  
91 [http://cdiac.ornl.gov/oceans/Moorings/Papa\\_145W\\_50N.html](http://cdiac.ornl.gov/oceans/Moorings/Papa_145W_50N.html), and some of the data were  
92 published by Fassbender et al. (2016). DIC was calculated using the total alkalinity (TA)- $p\text{CO}_2$   
93 pair in CO2sys program Version 1.1 (van Heuven et al. 2011), where TA was calculated using  
94 the linear relationship with salinity developed in Fassbender et al. (2016) ( $\text{TA} = 37 \times S + 988$ )  
95 for the OSP vicinity. The calculation was performed on the total pH scale using the carbonate  
96 dissociation constants ( $K_1'$  and  $K_2'$ ) of Lueker et al. (2000), the  $\text{HSO}_4^-$  dissociation constant from  
97 Dickson et al. (1990), and the  $B_T/S$  ratio from Lee et al. (2010). The DIC data were normalized  
98 to the annual mean salinity at OSP (32.5), to eliminate the influence from evaporation/dilution.

99 Water samples for phytoplankton abundance and community composition were collected  
100 at OSP during 14 Line P repeat hydrographic cruises aboard the CCGS John P. Tully from 2012  
101 to 2016 (February, June, and August for each year). Phytoplankton biomass, measured as total  
102 chlorophyll *a* (chl-*a*) concentrations, and the contribution of the main taxonomic groups of  
103 phytoplankton to chl-*a* were determined from high performance liquid chromatography (HPLC)

104 measurements of phytoplankton pigment concentrations (chlorophylls and carotenoids, Zapata  
105 et al. 2000) followed by CHEMTAX v1.95 analysis (Mackey et al., 1996). Eight algal groups  
106 were included in the chemotaxonomic analysis: diatoms, haptophytes, chlorophytes,  
107 pelagophytes, prasinophytes, dinoflagellates, cryptophytes, and cyanobacteria. However,  
108 cryptophytes were not found since their biomarker pigment, alloxanthin was not detected in any  
109 of our samples. Pigment ratios for each algal group were obtained from Higgins et al. (2011) and  
110 used as ‘seed’ values for multiple trials (60 runs) from randomized starting points, as described  
111 by Wright et al. (2009). The same initial pigment ratios (Table 1a) were used in all cruises but  
112 each cruise was run separately to allow potential variations in the CHEMTAX optimization to be  
113 expressed. The range of final pigment ratios are given in Table 1b and **the final ratios for each**  
114 **cruise are given in Peña et al. (2018)**. The six best solutions (those with the lowest residuals)  
115 were averaged for estimating the taxonomic abundances.

## 116 **2.2 Models used for NCP calculation**

### 117 **2.2.1 Oxygen mass balance model**

118 Oxygen, temperature, and salinity data from SOS-Argo F8397 and wind speed ( $U_{10}$ ) data  
119 from NOAA PMEL OSP mooring (<https://www.pmel.noaa.gov/ocs/data/disdell/>,  
120 <https://www.pmel.noaa.gov/ocs/data/fluxdissell/> ) were used in a multi-layer upper ocean  $O_2$   
121 mass balance model to calculate NCP. This model frame (Figure 3) is similar to what was used  
122 in Bushinsky and Emerson (2015), which compartmentalizes the upper ocean (0-150 m) into a  
123 mixed layer box (with variable height) with one meter boxes below. This model assumes that  
124 horizontal processes are not important. **Because horizontal gradients of oxygen are small**, lateral  
125 transport has much less influence on this property than fluxes from air-sea gas exchange, vertical  
126 advection, and diapycnal eddy diffusion. A detailed assessment of this assumption is given in

127 Yang et al. (2017). Furthermore, the temperature time series measured by the SOS-Argo (Figure  
128 S1) shows no significant intrusions of fronts/eddies, and the continuity of water mass during the  
129 study period also allows us to use this simplified model that ignores horizontal processes.

130 We define ANCP as the flux of organic carbon that escapes the “upper ocean” after a  
131 complete seasonal cycle. To be consistent with this definition NCP is integrated vertically from  
132 the surface ocean to the winter mixed layer depth, which in this location is roughly equal to the  
133 pycnocline depth. Because internal waves cause a 10 to 20 meter variation in the depth of density  
134 surfaces in this location, we used the annual mean pycnocline depth as the base of the modeled  
135 “upper ocean” to conserve mass in the model. Fluxes across the base of the upper ocean are  
136 calculated using measured gradients in oxygen at the density of the pycnocline, independent of  
137 its depth.

138 Oxygen concentration changes over time in the modeled “upper ocean” with depth of h  
139 ( $dh[O_2]/dt$ ) are the sum of: gas exchange fluxes ( $F_{A-W}$ ), vertical advection flux ( $F_V$ ), diapycnal  
140 eddy diffusion ( $F_{Kz}$ ), entrainment between the mixed layer and the water below ( $F_E$ ), and net  
141 biological oxygen production ( $J_{NCP}$ ).

$$\frac{dh[O_2]}{dt} = F_{A-W} + F_V + F_{Kz} + F_E + J_{NCP} \quad \text{mol m}^{-2} \text{d}^{-1} \quad (1)$$

142  
143  $F_{A-W}$  is calculated only for the mixed layer box, using the a gas exchange model that includes  
144 both diffusion and bubble processes (Emerson and Bushinsky, 2016; Liang et al., 2013). With  
145 the time step (3 h) used in our case, the mixed layer change between time steps is always smaller  
146 or equal to 1 m, so entrainment occurs only between the mixed layer box and the box below. The  
147 entrainment flux ( $F_E$ ) that gets out of the mixed layer box ends up going into the box below and  
148 vice versa, so  $F_E$  for these two boxes have the same value but different signs and cancel each

149 other out.  $F_V$  is calculated from Ekman pumping rate (derived from wind speed) and oxygen  
150 gradient from SOS-Argo measurements.  $F_{Kz}$  is calculated with oxygen gradient and diapycnal  
151 eddy diffusion coefficient from Cronin et al. (2015), which decreases with depth from the base of  
152 the mixed layer to a background value of  $10^{-5} \text{ m}^{-2} \text{ s}^{-1}$  (Whalen et al., 2012) with a  $1/e$  scaling  
153 described in Sun et al. (2013) (See also Bushinsky and Emerson, 2015). For the mixed layer  
154 reservoir  $F_{Kz}$  and  $F_V$  are considered only at the base of the box. For all the boxes below the mixed  
155 layer,  $F_{Kz}$  and  $F_V$  are considered both on the top and at the base of each box. Biological oxygen  
156 production,  $J_{NCP}$ , is the difference between the calculated fluxes and the measured time rate of  
157 change (left hand side of Equation 1). This value is converted from oxygen to carbon production  
158 (i.e. ANCP) using a constant oxygen to carbon ratio of 1.45 (Hedges et al., 2002).

159         The uncertainty of ANCP was estimated using a Monte Carlo approach. Confidence  
160 intervals for oxygen measurements and the gas exchange mass transfer coefficients used in the  
161 oxygen mass balance model were assigned to the model, and varied randomly while ANCP was  
162 calculated in two hundred runs for each calculation. Details of this approach are presented in the  
163 supporting information and Yang et al. (2017).

### 164 **2.2.2 DIC mass balance model**

165         We used a similar mass balance model for DIC, in which the base of the modeled “upper  
166 ocean” is set to the annual mean pycnocline depth (the same as the oxygen mass balance model).  
167 This choice of the upper ocean depth distinguishes this model from the mixed layer model used  
168 in Fassbender et al. (2016). Fluxes at the base of the upper ocean in our model use DIC  
169 gradients, diapycnal eddy diffusion coefficients, and upwelling velocities determined at the mean  
170 pycnocline depth while Fassbender et al. (2016) used the values at the bottom of the mixed layer.  
171 Because the OSP surface mooring provided only the mixed layer DIC data, we assumed that



172 there is no annual net DIC change in the depth region between the mixed layer and the annual  
173 mean pycnocline depth. The depth gradient of DIC used to calculate fluxes across the  
174 pycnocline was calculated from measured oxygen gradients assuming  $dO_2/dz$  to  $dDIC/dz$  ratio of  
175 1.45 (Hedges et al., 2002). Thus, we assume for this calculation that the DIC change at the  
176 pycnocline depth is only due to degradation of organic matter, which ignores the change due to  
177  $CaCO_3$  dissolution (Fassbender et al., 2016). For the DIC mass balance the multi-layer model is  
178 equivalent to a one-layer model:

$$\frac{dh[DIC]}{dt} = F_{A-W} + F_V + F_{Kz} + F_E + J_{NCP} \quad \text{mol m}^{-2} \text{d}^{-1} \quad (2)$$

179  
180 where the DIC change ( $dh[DIC]/dt$ ) for the modeled upper ocean (the air –sea interface to the  
181 mean depth of the pycnocline) is due to air-water  $CO_2$  exchange ( $F_{A-W}$ ) at the air-sea interface,  
182 vertical advection ( $F_V$ ) and diapycnal eddy diffusion ( $F_{Kz}$ ) at the base of the modeled “upper  
183 ocean”, and net biological carbon production ( $J_{NCP}$ ) in between. For this one-layer model,  
184 entrainment occurred within the same layer (box) and therefore there is no net entrainment flux  
185 ( $F_E = 0$ ). The air-sea gas-exchange mass transfer coefficient is calculated as a function of wind  
186 speed using equations from Wanninkhof (2014). The DIC gradients used for  $F_V$  and  $F_{Kz}$  are  
187 derived from oxygen gradients at the pycnocline depth as described above.

### 188 **2.3 Temperature dependence of NCP derived from the metabolic theory of ecology**

189 The correlation between NCP variation and environmental temperature could be  
190 attributed to the temperature dependence of planktonic metabolism. Regaudie-De-Gioux and  
191 Duarte (2012) derived the temperature dependences of gross primary production (GPP) and  
192 community respiration (CR) using the metabolic theory of ecology and a large historical dataset  
193 on volumetric planktonic metabolism in different seasons and ocean regimes (1156 estimates of

194 volumetric metabolic rates and the corresponding water temperature). Equations 3 & 4 below are  
 195 their linear regressions between the natural logarithm of the specific metabolic rates ( $GPP/Chla$   
 196 and  $CR/Chla$ ) and the inverted water temperature ( $1/kT$ ),

$$\ln \frac{GPP}{Chla} = a_p \frac{1}{kT} + b_p \quad (3)$$

$$\ln \frac{CR}{Chla} = a_r \frac{1}{kT} + b_r \quad (4)$$

197  
 198 where  $Chla$  is the chlorophyll- $a$  concentration,  $k$  is the Boltzmann's constant,  $T$  is the  
 199 environmental temperature in Kelvin, and  $a_p$ ,  $b_p$ ,  $a_r$ ,  $b_r$  are slopes and intercepts for each linear  
 200 regression. The temperature dependence of  $GPP/CR$  can be derived by combining Equations  
 201 3 & 4:

$$\frac{GPP}{CR} = EXP \left[ (a_p - a_r) \frac{1}{kT} + (b_p - b_r) \right] \quad (5)$$

202  
 203 Since the community respiration (CR) includes the respiration of both autotrophs and  
 204 heterotrophs, NCP can be calculated as the difference between GPP and CR.

$$NCP = GPP - CR = GPP \left( 1 - \frac{1}{\frac{GPP}{CR}} \right) \quad (6)$$

205 Combining Equations 5 and 6 gives us the NCP-temperature relationship.

$$NCP = GPP \left\{ 1 - \frac{1}{EXP \left[ (a_p - a_r) \frac{1}{kT} + (b_p - b_r) \right]} \right\} \quad (7)$$

206

## 207 **3 Results**

### 208 **3.1 Oxygen and DIC measurements**

209 The evolutions of density, oxygen concentration, and the oxygen anomaly in percent  
210 supersaturation ( $\Delta O_2 = ([O_2]/[O_2]_{\text{sat}} - 1) \times 100$ ) determined by the profiling float at OSP from 2012  
211 to 2016 are presented in Figure 4(a-c). The saturation concentration of oxygen ( $[O_2]_{\text{sat}}$ ) was  
212 calculated using equations from Garcia and Gordon (1992, 1993). The thin black line indicates  
213 the mixed layer depth, which is defined by a density offset from the value at 10 m using a  
214 threshold of  $0.03 \text{ kg m}^{-3}$  (de Boyer Montégut, 2004). The thick blue line indicates the pycnocline  
215 with a density of  $\sigma_\theta = 25.8 \text{ kg m}^{-3}$ , which follows  $[O_2]$  gradients well (Figure 4b). The white  
216 boxes indicate the modeled “upper ocean” for each year, in which base of the modeled “upper  
217 ocean” is the mean pycnocline depth for each year. Oxygen in the mixed layer was  
218 supersaturated from mid April to October/November, and near saturation or slightly  
219 undersaturated for the rest of the year (Figure 4c).

220 The evolution of salinity normalized DIC in the mixed layer determined by the OSP  
221 mooring is presented in Figure 4d. The  $p\text{CO}_2$  sensor stopped working during two periods in 2013  
222 and 2016 (indicated with dash line boxes), and therefore the data for these two periods is filled  
223 with interpolated values. Strong summertime DIC drawdown was observed in each year with the  
224 lowest DIC around September.

### 225 **3.2 Annual Net Community Production**

226 All the terms of the oxygen mass balance calculation in each year are presented in Table  
227 2a. The ANCP results ( $2.4 \pm 0.6$ ,  $0.8 \pm 0.4$ ,  $2.1 \pm 0.4$  and  $1.6 \pm 0.4 \text{ mol C m}^{-2} \text{ yr}^{-1}$ , with a mean  
228 value of  $1.7 \pm 0.7 \text{ mol C m}^{-2} \text{ yr}^{-1}$ ) indicate that ANCP initially decreased after warmer water  
229 invaded this area (2013-14) and then returned to the “pre-blob” value of 2012-13 in subsequent  
230 years. Given the uncertainty in the estimate of ANCP in each year, the value during year 2013-  
231 14 is significantly different at the 95% confidence interval (as determined by t-test, Bethea et al.,

232 1975). With the exception of the unusually low value for 2013-14, ANCP values from oxygen  
233 mass balance calculation are very close to the historical ANCP estimates at OSP ( $2.3 \pm 0.6$  mol  
234  $\text{C m}^{-2} \text{ yr}^{-1}$ , Emerson 2014).

235 If we integrate the ANCP from the ocean surface to the depth of the mixed layer  
236 ( $\text{ANCP}_{\text{mixed layer}}$  in Table 2a) instead of to the annual mean depth of the pycnocline, the results are  
237 higher ( 3.4, 1.3, 2.3 and 2.3 mol  $\text{C m}^{-2} \text{ yr}^{-1}$ , with a mean value of  $2.4 \pm 0.9$  mol  $\text{C m}^{-2} \text{ yr}^{-1}$ ).  
238 While the mean value is higher because it includes some organic carbon flux that is degraded  
239 between the mixed layer and pycnocline in summer, the annual trend, in which ANCP is  
240 significantly lower in year two (2013-14), is the same as that in which ANCP values were  
241 determined for the depth interval above the pycnocline.

242 In comparison, ANCP values determined from DIC mass balance are 2.0, 2.1, 2.6, 3.0  
243 mol  $\text{C m}^{-2} \text{ yr}^{-1}$ , with a mean value of  $2.4 \pm 0.5$  mol  $\text{C m}^{-2} \text{ yr}^{-1}$  (Table 2b). The mean value is  
244 similar within the errors of the value determined from the oxygen mass balance ( $1.7 \pm 0.7$  mol  $\text{C}$   
245  $\text{m}^{-2} \text{ yr}^{-1}$ ) but there is no significant change between the second year (2013-14) and those before  
246 and after. The somewhat higher value could be due to the assumption we made about DIC  
247 change below the mixed layer or because we neglected horizontal advection (See Discussion).

### 248 **3.3 Phytoplankton abundance and community composition**

249 *Chl-a* concentration, an indicator of phytoplankton biomass, was about 50% lower (0.22  
250  $\text{mg m}^{-3}$ ) during the period from August 2013 to June 2014 than during the rest of the 2012 to  
251 2016 period (Figure 5a) and the historical annual average at OSP (Peña and Varela, 2007). *Chl-a*  
252 resumed to the 2012-13 level in August 2014 and had a significant increase in the summer of  
253 2016. 19'-hexanoyloxyfucoxanthin (Hex), which is mainly derived from prymnesiophytes, was  
254 found to be the most abundant pigment after T-*chl-a* (Figure 5b). Fucoxanthin (Fuco), a pigment

255 associated with diatoms, haptophytes and pelagophytes, was also abundant and showed increased  
256 concentration ( $0.54 \text{ mg m}^{-3}$ ) in June 2016, coinciding with increased T-chla. After Hex, and  
257 Fuco, chlorophyll-b was the most abundant pigment ( $0.36$  to  $0.27 \text{ mg m}^{-3}$ ), indicating the  
258 presence of green algae. We also detected occasionally lutein ( $0$ - $0.125 \text{ mg m}^{-3}$ ), violaxanthin ( $0$ -  
259  $0.012 \text{ mg m}^{-3}$ ) and, prasinoxanthin ( $0$ - $0.005 \text{ mg m}^{-3}$ ), which are biomarkers for green algae.

260 The CHEMTAX analysis detected the presence of seven classes of phytoplankton  
261 (Figure 5c) and showed an increase in the relative contribution of cyanobacteria and  
262 chlorophytes during the “Blob” period with the highest proportion of the former group in June of  
263 2014 and the latter in June 2015 (Figure 5c). There was also a decrease in the abundance of  
264 diatoms from August 2013 to June 2015. The remainder of the phytoplankton community was  
265 primarily composed of haptophytes and the contribution of the other phytoplankton groups was  
266 variable and showed no consistent year-to-year variability. By August 2015 the phytoplankton  
267 community had returned to a similar relative composition as observed in 2012-13, with  
268 nanoplankton (mostly haptophytes) being dominant and with microplankton (diatoms and  
269 dinoflagellates) increasing in abundance. The input matrix (Table 1a) appeared to describe the  
270 environment well since the final pigment ratio matrix did not differ dramatically from the initial  
271 input values.

## 272 **4 Discussion**

### 273 **4.1 Comparisons of ANCP from oxygen and DIC mass balances**

274 Although the ANCP are integrated to the same depth in our oxygen and DIC mass  
275 balance models, as mentioned in Section 3.2, the ANCP determined from DIC mass balance (4-  
276 year mean:  $2.4 \pm 0.5 \text{ mol C m}^{-2} \text{ yr}^{-1}$ ) is somewhat higher than the value determined from oxygen  
277 mass balance (4-year mean:  $1.7 \pm 0.7 \text{ mol C m}^{-2} \text{ yr}^{-1}$ ), but still within the error of the model.

278 There are two possible reasons for such discrepancy. First of all, due to the lack of DIC data  
279 below the mixed layer, for the DIC model we made an assumption that there is no annual net  
280 DIC change in the depth region between the mixed layer and the annual mean pycnocline depth.  
281 With this assumption, the ANCP from DIC mass balance is higher because it includes the  
282 organic carbon that is degraded between the mixed layer and pycnocline in summer, so the  
283 ANCP from DIC mass balance (4-year mean:  $2.4 \pm 0.5 \text{ mol C m}^{-2} \text{ yr}^{-1}$ ) is very similar to the  
284 mixed layer ANCP determined from our oxygen mass balance model (4-year mean:  $2.4 \pm 0.9$   
285  $\text{mol C m}^{-2} \text{ yr}^{-1}$ ) and the mixed layer ANCP determined by Fassbender et al. (2016) ( $2 \pm 1 \text{ mol C}$   
286  $\text{m}^{-2} \text{ yr}^{-1}$ ). The second possible reason that the 4-year mean value of ANCP determined from the  
287 DIC mass balance is higher than the value determined from the oxygen mass balance is  
288 horizontal advection. Because gas exchange resets the oxygen saturation anomaly for oxygen  
289 about ten times faster than  $\text{CO}_2$ , the DIC mass balance is more vulnerable to horizontal fluxes  
290 than the  $\text{O}_2$  mass balance. If we assumed that the difference in ANCP estimated from these two  
291 tracers ( $0.7 \text{ mol C m}^{-2} \text{ yr}^{-1}$ ) is due to horizontal advection, and calculate the horizontal DIC  
292 gradient using the 4-year mean horizontal velocity at OSP of  $0.08 \text{ m s}^{-1}$ , we found that a  
293 horizontal DIC gradient of  $1 \times 10^{-8} \text{ mol m}^{-4}$  is required to cause the difference of  $0.7 \text{ mol C m}^{-2} \text{ yr}^{-1}$   
294 <sup>1</sup>, which is possible at this location (horizontal DIC gradient along the 4-year mean horizontal  
295 flow at OSP is about  $2 \sim 3 \times 10^{-8} \text{ mol m}^{-4}$  from GLODAP v1.1 gridded product, Key et al., 2004).

296 As for the inter-annual changes in ANCP, the oxygen mass balance calculation shows  
297 that ANCP had a significant decrease in 2013-14 and then returned to the “pre-blob” level in the  
298 following years whereas ANCP calculated from DIC mass balance does not show this trend.  
299 Since air-sea exchange is a large part of the flux mass balance for both oxygen and  $\text{CO}_2$  (Table  
300 2), a likely reason for this discrepancy is due to the shorter residence time with respect to gas

301 exchange for the oxygen compared to the CO<sub>2</sub> saturation anomalies. An example of the residence  
302 time calculation is included in the supporting information where it indicates that the gas  
303 exchange residence time in the upper ocean for oxygen is about one month and that for CO<sub>2</sub> is  
304 about one year (See also Emerson and Hedges, 2008, Chapter 11). Thus, the biologically induced  
305 saturation anomaly for oxygen responds fast enough to record annual changes whereas that for  
306 *p*CO<sub>2</sub> and DIC does not. On the other hand, as discussed above, since DIC mass balance is more  
307 vulnerable to horizontal flux than oxygen mass balance, the DIC signal might already been  
308 “smoothed” by the horizontal flux, which may also explain why the inter-annual ANCP changes  
309 were not observed by using the DIC mass balance approach. Alternatively, the production ratio  
310 of particulate organic carbon (POC) and particulate inorganic carbon (PIC) may cause the inter-  
311 annual variation of DIC mass balance. However, in our case since there was no significant bloom  
312 of haptophytes (e.g. coccolithophore) during the study period (Figure 5c), it is unlikely that the  
313 inter-annual change in POC/PIC ratio would affect the ANCP result calculated from DIC mass  
314 balance. The sharp decrease in ANCP from the oxygen mass balance in 2013-14 is consistent  
315 with the decrease in chlorophyll concentration by about 50% observed for the same period  
316 (Figure 5a). Hence, from this point forward we will focus on analyzing the factors that might  
317 influence ANCP variations determined by the oxygen mass balance model.

#### 318 **4.2 Causes of ANCP decrease**

319 In the following paragraphs, we analyze connections between ANCP decrease and the  
320 “Blob” temperature anomaly in the context of multiple physical and biological processes,  
321 including the choices of start time from which ANCP are calculated, the base depth of the  
322 modeled “upper ocean”, planktonic metabolism, and changes in phytoplankton community  
323 composition.

324 Our observations began in June 2012, 10 – 12 months before the positive SST anomalies.  
325 To determine whether the start date for determining the ANCP values affects the results, we  
326 began the time series on four different months (Table 3). We are somewhat limited because  
327 there is only about 12 “pre-blob” months before June, 2012. However, as shown in Table 3, as  
328 long as there are more “pre-blob” months than “Blob-affected” months in the 1<sup>st</sup> year, the  
329 significant ANCP decrease from 1<sup>st</sup> to 2<sup>nd</sup> year is still observed and the trend of ANCP variation  
330 for those 4 years remains.

331 To determine whether the annual mean pycnocline depth (the white rectangles in Figure  
332 4a-4c) influences the ANCP trends we calculated ANCP using the 4-year mean depth of 100 m  
333 for the modeled “upper ocean”. The ANCP results only change slightly (2.6, 1.0, 1.9, and 1.6  
334 mol C m<sup>-2</sup> yr<sup>-1</sup>) and the decrease in 2013-14 is still statistically significant, indicating that the  
335 different base depth used for the modeled “upper ocean” is not the key factor that causes ANCP  
336 changes.

337 To test if the temperature dependence of planktonic metabolism is strong enough to  
338 cause the ANCP decline we observed (e.g. 1.6 mol C m<sup>-2</sup> yr<sup>-1</sup> between 2012-13 and 2013-14), we  
339 calculated the GPP from measured NCP of year 1 (2012-13) using Equation 7, and assumed GPP  
340 was constant for all four years so we could then determine the effect of temperature on NCP  
341 based on the metabolic theory of ecology (Equation 7). Since the specific phytoplankton growth  
342 rate increases with increasing temperature (e.g. Regaudie-De-Gioux and Duarte, 2012; Chen and  
343 Laws, 2017), if phytoplankton biomass would have remained the same during the “blob”, GPP  
344 would have increased. Thus, assuming a constant GPP in this calculation is somewhat  
345 speculative, but it at least provides a first order assessment of the metabolic temperature effect on  
346 ANCP. The parameterizations derived with datasets from Arctic were used (Regaudie-De-Gioux



347 and Duarte, 2012), because it gives the largest change in ANCP. The results (Table 4) indicate  
348 that temperature dependence of planktonic metabolism is not strong enough to account for the  
349 measured ANCP decrease in the 2<sup>nd</sup> year (2013-14), suggesting that this is not the major reason  
350 for the observed ANCP decline.

351 Having ruled out the above likely candidates, we suggest that the low phytoplankton  
352 biomass observed in the 2<sup>nd</sup> year (2013-14, Figure 5a), and the observed change in phytoplankton  
353 community composition (Figure 5c) are the most likely causes for the ANCP decrease. In  
354 general, larger phytoplankton (i.e. microplankton) are more efficient exporters than smaller  
355 nanoplankton and picoplankton (e.g., Chen and Laws, 2016). Given the lower export rates of  
356 picoplankton (e.g. cyanobacteria) than those of larger phytoplankton (e.g. diatoms) the observed  
357 changes in phytoplankton community composition (Figure 5b) in 2013-14, which included a  
358 decrease in the relative abundance of diatoms, and an increase in the relative abundance of  
359 cyanobacteria and green algae (chlorophytes), could have further contributed to the decrease in  
360 ANCP. After the initial response to the temperature anomaly, chl-*a* concentration and the  
361 phytoplankton community composition returned to a level similar to those observed before the  
362 warming occurred, suggesting that the plankton community rapidly adapted to the higher  
363 temperature and prevailing environmental conditions. These changes in phytoplankton  
364 community composition could be ultimately in response to the lack of micronutrients like iron  
365 (due to enhanced stratification from the “blob” that restricted the vertical supply), which has  
366 been shown to regulate phytoplankton biomass and composition in this high-nutrient low-  
367 chlorophyll region (e.g. Hamme et al., 2010; Marchetti et al., 2006), . Unfortunately, we do not  
368 have iron data available to confirm that at this time.

## 369 **5 Conclusions**

370 The annual net community production (ANCP) at Ocean Station Papa (OSP) in the  
371 subarctic Northeast Pacific Ocean was determined from June 2012 to June 2016 to examine the  
372 effect of the temperature anomaly on the efficiency of carbon export. The ANCP determined by  
373 oxygen mass balance had a four year mean value of  $1.7 \pm 0.7 \text{ mol C m}^{-2} \text{ yr}^{-1}$ , whereas ANCP  
374 determined by DIC mass balance gives a somewhat higher mean value ( $2.4 \pm 0.5 \text{ mol C m}^{-2} \text{ yr}^{-1}$ ).  
375 ANCP for individual years determined from O<sub>2</sub> mass balance showed a significant decrease in  
376 year 2 (2013-14) after the onset of the temperature anomaly, but no significant decrease in  
377 ANCP was found when calculated with DIC mass balance. We believe that this indicates that  
378 the DIC concentration and *p*CO<sub>2</sub> respond too slowly to capture annual changes in ANCP. Based  
379 on our observations and historical ANCP estimates at OSP as reference, we found there was a  
380 significant ANCP decrease in 2013-14 due to the warm anomaly, which is consistent with the  
381 findings from concurrent phytoplankton data. Possible mechanisms for the observed decrease in  
382 ANCP by the oxygen mass balance in the second year were analyzed in the context of multiple  
383 physical and biological processes that could be affected by temperature anomaly. Our analysis  
384 showed that the ANCP decrease was most likely due to changes in phytoplankton abundance and  
385 community composition after the “Blob” entered the area.

386

387 ***Data availability.***

388 Float data are available online (<https://sites.google.com/a/uw.edu/sosargo/home>). Mooring data  
389 is available online at: [http://cdiac.ornl.gov/oceans/Moorings/Papa\\_145W\\_50N.html](http://cdiac.ornl.gov/oceans/Moorings/Papa_145W_50N.html).

390 ***Author contributions.***

391 BY and SRE designed the experiments. BY developed the model code and process the data. AP  
392 provided the data, analysis and interpretation of phytoplankton. BY and SRE prepared the  
393 manuscript with contributions from all co-authors.

#### 394 *Competing interests.*

395 The authors declare that they have no conflict of interest.

#### 396 *Acknowledgements.*

397 We thank Dr. Stephen Riser and Dana Swift for their assistance in development of the SOS-Argo  
398 float, and scientists of NOAA PMEL and the Institute of Ocean Sciences (IOS) and crews of  
399 CCGS John P. Tully, for their work on OSP mooring and Line P cruises. Special thanks are  
400 given to Dr. John Crusius for the constructive discussions and comments on this study. This  
401 work was supported by National Science Foundation grant OCE-1458888.

#### 402 **References**

- 403 Allen, A. P., Gillooly, J. F. and Brown, J. H.: Linking the global carbon cycle to individual  
404 metabolism, *Funct. Ecol.*, 19(2), 202–213, doi:10.1111/j.1365-2435.2005.00952.x, 2005.
- 405 Bethea, R. M., Duran, B. S. and Boullion, T. L.: *Statistical methods for engineers and scientists*,  
406 Marcel Dekker, Inc., New York., 1975.
- 407 Bond, N. A., Cronin, M. F., Freeland, H. and Mantua, N.: Causes and impacts of the 2014 warm  
408 anomaly in the NE Pacific, *Geophys. Res. Lett.*, 42(9), 3414–3420, doi:10.1002/2015GL063306,  
409 2015.
- 410 de Boyer Montégut, C.: Mixed layer depth over the global ocean: An examination of profile data  
411 and a profile-based climatology, *J. Geophys. Res.*, 109(C12), C12003,  
412 doi:10.1029/2004JC002378, 2004.
- 413 Brown, J. H., Gillooly, J. F., Allen, A. P., Savage, V. M. and West, G. B.: TOWARD A  
414 METABOLIC THEORY OF ECOLOGY, *Ecology*, 85(7), 1771–1789, doi:10.1890/03-9000,  
415 2004.
- 416 Bushinsky, S. M. and Emerson, S.: Marine biological production from in situ oxygen  
417 measurements on a profiling float in the subarctic Pacific Ocean, *Global Biogeochem. Cycles*,  
418 29(12), 2050–2060, 2015.
- 419 Bushinsky, S. M., Emerson, S. R., Riser, S. C. and Swift, D. D.: Accurate oxygen measurements  
420 on modified Argo floats using in situ air calibrations, *Limnol. Oceanogr. Methods*, 2016.
- 421 Cavole, L., Demko, A., Diner, R., Giddings, A., Koester, I., Pagniello, C., Paulsen, M.-L.,  
422 Ramirez-Valdez, A., Schwenck, S., Yen, N., Zill, M. and Franks, P.: Biological Impacts of the  
423 2013–2015 Warm-Water Anomaly in the Northeast Pacific: Winners, Losers, and the Future,  
424 *Oceanography*, 29(2), 273–285, doi:10.5670/oceanog.2016.32, 2016.

425 Charette, M. A., Bradley Moran, S. and Bishop, J. K. B.: as a tracer of particulate organic carbon  
426 export in the subarctic northeast Pacific Ocean, *Deep Sea Res. Part II Top. Stud. Oceanogr.*,  
427 46(11–12), 2833–2861, doi:10.1016/S0967-0645(99)00085-5, 1999.

428 Chen, B. and Laws, E. A.: Is there a difference of temperature sensitivity between marine  
429 phytoplankton and heterotrophs?, *Limnol. Oceanogr.*, doi:10.1002/lno.10462, 2016.

430 Cronin, M. F., Pelland, N. A., Emerson, S. R. and Crawford, W. R.: Estimating diffusivity from  
431 the mixed layer heat and salt balances in the North Pacific, *J. Geophys. Res. Ocean.*, 120(11),  
432 7346–7362, 2015.

433 Dickson, A. G., Wesolowski, D. J., Palmer, D. A. and Mesmer, R. E.: Dissociation constant of  
434 bisulfate ion in aqueous sodium chloride solutions to 250. degree. C, *J. Phys. Chem.*, 94(20),  
435 7978–7985, 1990.

436 Emerson, S.: Seasonal oxygen cycles and biological new production in surface waters of the  
437 subarctic Pacific Ocean, *J. Geophys. Res. Ocean.*, 92(C6), 6535–6544, 1987.

438 Emerson, S. and Bushinsky, S.: The role of bubbles during air-sea gas exchange, *J. Geophys.*  
439 *Res. Ocean.*, 2016.

440 Emerson, S. and Hedges, J.: Chemical oceanography and the marine carbon cycle., 2008.

441 Emerson, S. and Stump, C.: Net biological oxygen production in the ocean—II: Remote in situ  
442 measurements of O<sub>2</sub> and N<sub>2</sub> in subarctic pacific surface waters, *Deep Sea Res. Part I Oceanogr.*  
443 *Res. Pap.*, 57(10), 1255–1265, 2010.

444 Emerson, S., Quay, P., Stump, C., Wilbur, D. and Knox, M.: O<sub>2</sub>, Ar, N<sub>2</sub>, and <sup>222</sup>Rn in surface  
445 waters of the subarctic Ocean: Net biological O<sub>2</sub> production, *Global Biogeochem. Cycles*, 5(1),  
446 49–69, doi:10.1029/90GB02656, 1991.

447 Emerson, S., Quay, P. and Wheeler, P. A.: Biological productivity determined from oxygen mass  
448 balance and incubation experiments, *Deep Sea Res. Part I Oceanogr. Res. Pap.*, 40(11), 2351–  
449 2358, 1993.

450 Emerson, S., Sabine, C., Cronin, M. F., Feely, R., Cullison Gray, S. E. and DeGrandpre, M.:  
451 Quantifying the flux of CaCO<sub>3</sub> and organic carbon from the surface ocean using in situ  
452 measurements of O<sub>2</sub>, N<sub>2</sub>, pCO<sub>2</sub>, and pH, *Global Biogeochem. Cycles*, 25(3), n/a-n/a,  
453 doi:10.1029/2010GB003924, 2011.

454 Fassbender, A. J., Sabine, C. L. and Cronin, M. F.: Net community production and calcification  
455 from 7 years of NOAA Station Papa Mooring measurements, *Global Biogeochem. Cycles*, 30(2),  
456 250–267, doi:10.1002/2015GB005205, 2016.

457 Freeland, H.: A short history of Ocean Station Papa and Line P, *Prog. Oceanogr.*, 75(2), 120–  
458 125, doi:10.1016/j.pocean.2007.08.005, 2007.

459 Freeland, H. J. and Cummins, P. F.: Argo: A new tool for environmental monitoring and  
460 assessment of the world’s oceans, an example from the N.E. Pacific, *Prog. Oceanogr.*, 64(1), 31–  
461 44, doi:10.1016/j.pocean.2004.11.002, 2005.

462 Garcia, H. E. and Gordon, L. I.: Oxygen solubility in seawater: Better fitting equations, *Limnol.*  
463 *Oceanogr.*, 37(6), 1307–1312, doi:10.4319/lo.1992.37.6.1307, 1992.

464 Garcia, H. E. and Gordon, L. I.: Erratum: Oxygen Solubility in Seawater: Better Fitting  
465 Equations, *Limnol. Oceanogr.*, 38(3), 656 [online] Available from:  
466 <http://www.jstor.org/stable/2838040?seq=1>, 1993.

467 Giesbrecht, K. E., Hamme, R. C. and Emerson, S. R.: Biological productivity along Line P in the  
468 subarctic northeast Pacific: In situ versus incubation-based methods, *Global Biogeochem.*  
469 *Cycles*, 26(3), doi:10.1029/2012GB004349, 2012.

470 Gillooly, J. F., Brown, J. H. and West, G. B.: Effects of Size and Temperature on Metabolic

471 Rate, *Science* (80-.), 293(September), 2248–2252, doi:10.1126/science.1061967, 2001.  
472 Hamme, R. C., Webley, P. W., Crawford, W. R., Whitney, F. A., Degrandpre, M. D., Emerson,  
473 S. R., Eriksen, C. C., Giesbrecht, K. E., Gower, J. F. R., Kavanaugh, M. T., Pea, M. A., Sabine,  
474 C. L., Batten, S. D., Coogan, L. A., Grundle, D. S. and Lockwood, D.: Volcanic ash fuels  
475 anomalous plankton bloom in subarctic northeast Pacific, *Geophys. Res. Lett.*, 37(19),  
476 doi:10.1029/2010GL044629, 2010.  
477 Hedges, J. I., Baldock, J. A., G??linas, Y., Lee, C., Peterson, M. L. and Wakeham, S. G.: The  
478 biochemical and elemental compositions of marine plankton: A NMR perspective, *Mar. Chem.*,  
479 78(1), 47–63, doi:10.1016/S0304-4203(02)00009-9, 2002.  
480 van Heuven, S., Pierrot, D., Rae, J. W. B., Lewis, E. and Wallace., D. W. R.: MATLAB Program  
481 Developed for CO2 System Calculations. ORNL/CDIAC-105b., ,  
482 doi:10.3334/CDIAC/otg.CO2SYS\_MATLAB\_v1.1, 2011.  
483 Johnson, K. S., Berelson, W. M., Boss, E. S., Claustre, H., Emerson, S. R., Gruber, N.,  
484 Körtzinger, A., Perry, M. J. and Riser, S. C.: Observing Biogeochemical Cycles at Global Scales  
485 with Profiling Floats and Gliders: Prospects for a Global Array, *Oceanography*, 22 [online]  
486 Available from: <http://dx.doi.org/10.5670/oceanog.2009.81>, 2009.  
487 Juranek, L. W., Quay, P. D., Feely, R. A., Lockwood, D., Karl, D. M. and Church, M. J.:  
488 Biological production in the NE Pacific and its influence on air-sea CO2 flux: Evidence from  
489 dissolved oxygen isotopes and O2/Ar, *J. Geophys. Res. Ocean.*, 117(C5), n/a-n/a,  
490 doi:10.1029/2011jc007450, 2012.  
491 Key, R. M., Kozyr, A., Sabine, C. L., Lee, K., Wanninkhof, R., Bullister, J. L., Feely, R. A.,  
492 Millero, F. J., Mordy, C. and Peng, T. H.: A global ocean carbon climatology: Results from  
493 Global Data Analysis Project (GLODAP), *Global Biogeochem. Cycles*, 18(4), 1–23,  
494 doi:10.1029/2004GB002247, 2004.  
495 Lee, K., Kim, T.-W., Byrne, R. H., Millero, F. J., Feely, R. A. and Liu, Y.-M.: The universal  
496 ratio of boron to chlorinity for the North Pacific and North Atlantic oceans, *Geochim.*  
497 *Cosmochim. Acta*, 74(6), 1801–1811, 2010.  
498 Liang, J. H., Deutsch, C., McWilliams, J. C., Baschek, B., Sullivan, P. P. and Chiba, D.:  
499 Parameterizing bubble-mediated air-sea gas exchange and its effect on ocean ventilation, *Global*  
500 *Biogeochem. Cycles*, 27(3), 894–905, doi:10.1002/gbc.20080, 2013.  
501 López-Urrutia, A., San Martin, E., Harris, R. P. and Irigoien, X.: Scaling the metabolic balance  
502 of the oceans., *Proc. Natl. Acad. Sci. U. S. A.*, 103(23), 8739–44, doi:10.1073/pnas.0601137103,  
503 2006.  
504 Di Lorenzo, E. and Mantua, N.: Multi-year persistence of the 2014/15 North Pacific marine  
505 heatwave, *Nat. Clim. Chang.*, (July), 1–7, doi:10.1038/nclimate3082, 2016.  
506 Lueker, T. J., Dickson, A. G. and Keeling, C. D.: Ocean pCO2 calculated from dissolved  
507 inorganic carbon, alkalinity, and equations for K1 and K2: validation based on laboratory  
508 measurements of CO2 in gas and seawater at equilibrium, *Mar. Chem.*, 70(1), 105–119, 2000.  
509 Mackey, M. D., Mackey, D. J., Higgins, H. W. and Wright, S. W.: CHEMTAX - A program for  
510 estimating class abundances from chemical markers: Application to HPLC measurements of  
511 phytoplankton, *Mar. Ecol. Prog. Ser.*, 144(1–3), 265–283, doi:10.3354/meps144265, 1996.  
512 Marchetti, A., Juneau, P., Whitney, F. A., Wong, C. S. and Harrison, P. J.: Phytoplankton  
513 processes during a mesoscale iron enrichment in the NE subarctic Pacific: Part II-Nutrient  
514 utilization, *Deep. Res. Part II Top. Stud. Oceanogr.*, 53(20–22), 2114–2130,  
515 doi:10.1016/j.dsr2.2006.05.031, 2006.  
516 Peña, M. A. and Varela, D. E.: Seasonal and interannual variability in phytoplankton and nutrient

517 dynamics along Line P in the NE subarctic Pacific, *Prog. Oceanogr.*, 75(2), 200–222,  
518 doi:10.1016/j.pocean.2007.08.009, 2007.

519 Peña, M. A., Nemcek, N. and Robert, M.: Phytoplankton responses to the 2014-2016 warming  
520 anomaly in the Northeast Subarctic Pacific Ocean, *Limnol. Oceanogr.*, in press, 2018.

521 Plant, J. N., Johnson, K. S., Sakamoto, C. M., Jannasch, H. W., Coletti, L. J., Riser, S. C. and  
522 Swift, D. D.: Net community production at Ocean Station Papa observed with nitrate and oxygen  
523 sensors on profiling floats, *Global Biogeochem. Cycles*, 30(6), 859–879,  
524 doi:10.1002/2015GB005349, 2016.

525 Regaudie-De-Gioux, A. and Duarte, C. M.: Temperature dependence of planktonic metabolism  
526 in the ocean, *Global Biogeochem. Cycles*, 26(1), doi:10.1029/2010GB003907, 2012.

527 Rose, J. M. and Caron, D. A.: Does low temperature constrain the growth rates of heterotrophic  
528 protists? Evidence and implications for algal blooms in cold waters, *Limnol. Oceanogr.*, 52(2),  
529 886–895, doi:10.4319/lom.2007.52.2.0886, 2007.

530 Sun, O. M., Jayne, S. R., Polzin, K. L., Rahter, B. A. and St. Laurent, L. C.: Scaling Turbulent  
531 Dissipation in the Transition Layer, *J. Phys. Oceanogr.*, 43(11), 2475–2489, doi:10.1175/JPO-D-  
532 13-057.1, 2013.

533 Takahashi, T., Olafsson, J., Goddard, J. G., Chipman, D. W. and Sutherland, S. C.: Seasonal  
534 variation of CO<sub>2</sub> and nutrients in the high-latitude surface oceans: A comparative study, *Global  
535 Biogeochem. Cycles*, 7(4), 843–878, doi:10.1029/93GB02263, 1993.

536 Wanninkhof, R.: Relationship between wind speed and gas exchange over the ocean revisited,  
537 *Limnol. Oceanogr. Methods*, 12(JUN), 351–362, doi:10.4319/lom.2014.12.351, 2014.

538 Whalen, C. B., Talley, L. D. and MacKinnon, J. A.: Spatial and temporal variability of global  
539 ocean mixing inferred from Argo profiles, *Geophys. Res. Lett.*, 39(17),  
540 doi:10.1029/2012GL053196, 2012.

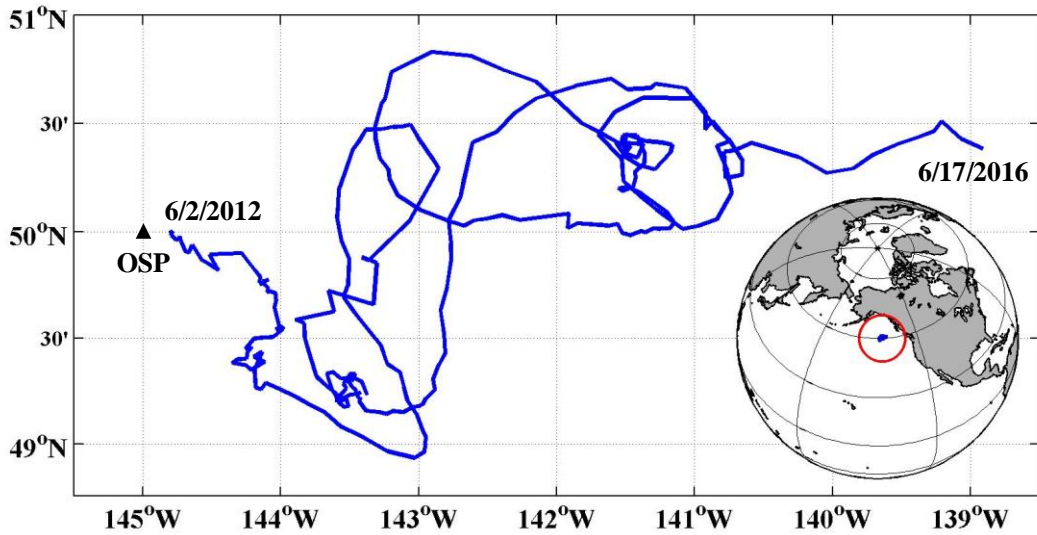
541 Wong, C. S., Waser, N. A. D., Nojiri, Y., Whitney, F. A., Page, J. S. C. and Zeng, J.: Seasonal cycles of  
542 nutrients and dissolved inorganic carbon at high and mid latitudes in the North Pacific Ocean  
543 during the Skaugran cruises: determination of new production and nutrient uptake ratios, *Deep  
544 Sea Res. Part II Top. Stud. Oceanogr.*, 49(24–25), 5317–5338, doi:10.1016/S0967-  
545 0645(02)00193-5, 2002a.

546 Wong, C. S.: Analysis of trends in primary productivity and chlorophyll-a over two decades at  
547 Ocean Station P (50°N, 145°W) in the subarctic northeast Pacific Ocean, *Can. J. Fish. Aquat.  
548 Sci.*, 121, 107–117 [online] Available from: <http://ci.nii.ac.jp/naid/10009665016/en/> (Accessed 4  
549 February 2017), 1995.

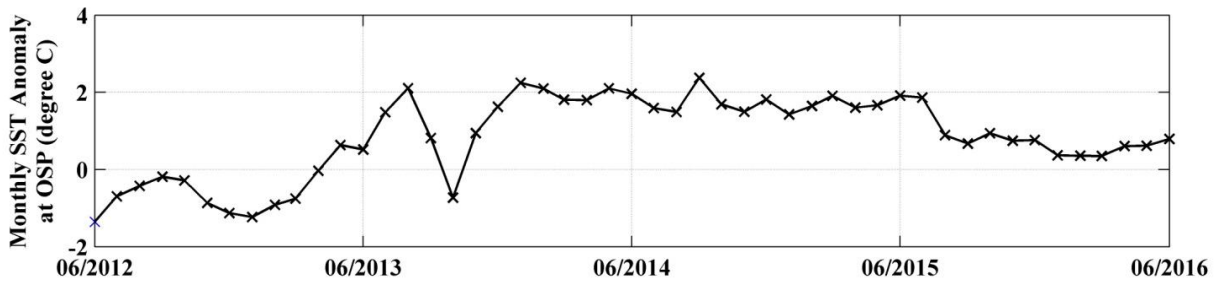
550 Wong, C. S., Waser, N. A. D., Nojiri, Y., Johnson, W. K., Whitney, F. A., Page, J. S. C. and  
551 Zeng, J.: Seasonal and Interannual Variability in the Distribution of Surface Nutrients and  
552 Dissolved Inorganic Carbon in the Northern North Pacific: Influence of El Niño, *J. Oceanogr.*,  
553 58(2), 227–243, doi:10.1023/A:1015897323653, 2002b.

554 Yang, B., Emerson, S. R. and Bushinsky, S. M.: Annual net community production in the  
555 subtropical Pacific Ocean from in-situ oxygen measurements on profiling floats., *Global  
556 Biogeochem. Cycles*, doi:10.1002/2016GB005545, 2017.

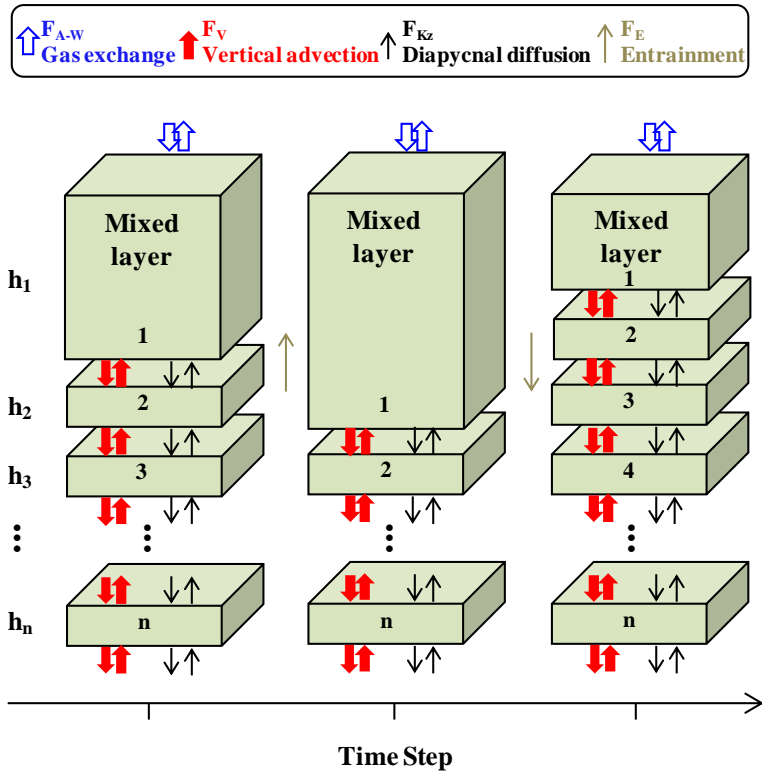
557 Zapata, M., F. Rodrigues, and J. L. Garrido. 2000. Separation of chlorophylls and carotenoids  
558 from marine phytoplankton: a new HPLC method using a reversed phase C-8 column and  
559 pyridine-containing mobile phases. *Mar. Ecol. Prog. Ser.* **195**: 29–45. doi:10.3354/meps195029.  
560



561  
 562 **Figure 1** Study area and float path from 2012 to 2016. The black triangle indicates the position  
 563 of Ocean Station Papa (OSP) Mooring, and the blue line indicates the trajectory of the SOS-Argo  
 564 float which was within roughly a  $2^{\circ}$  (N-S)  $\times$   $6^{\circ}$  (E-W) box.  
 565



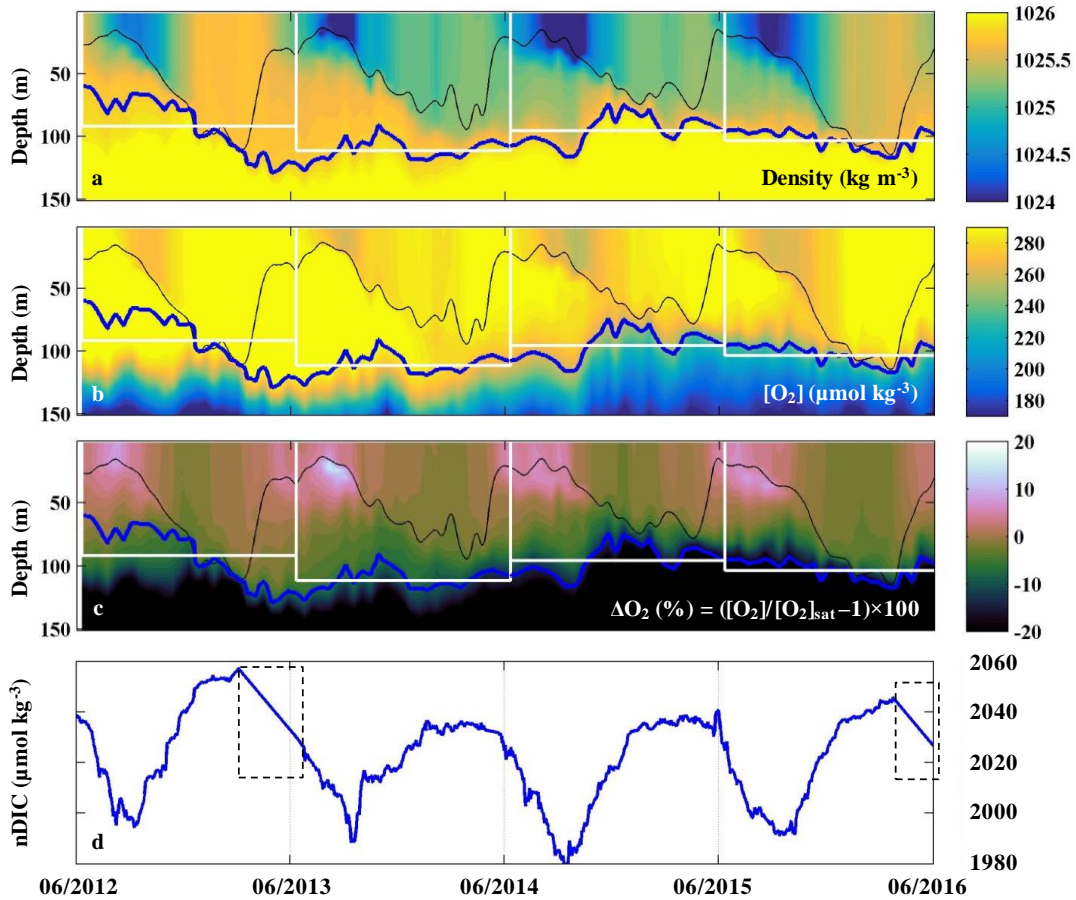
566  
 567 **Figure 2** Monthly SST Anomaly at Ocean Station Papa (OSP). The anomaly is defined as the  
 568 difference between the measured SST and the mean of 1971-2000. Data are from:  
 569 [http://iridl.ldeo.columbia.edu/maproom/Global/Ocean\\_Temp/Anomaly.html](http://iridl.ldeo.columbia.edu/maproom/Global/Ocean_Temp/Anomaly.html)  
 570



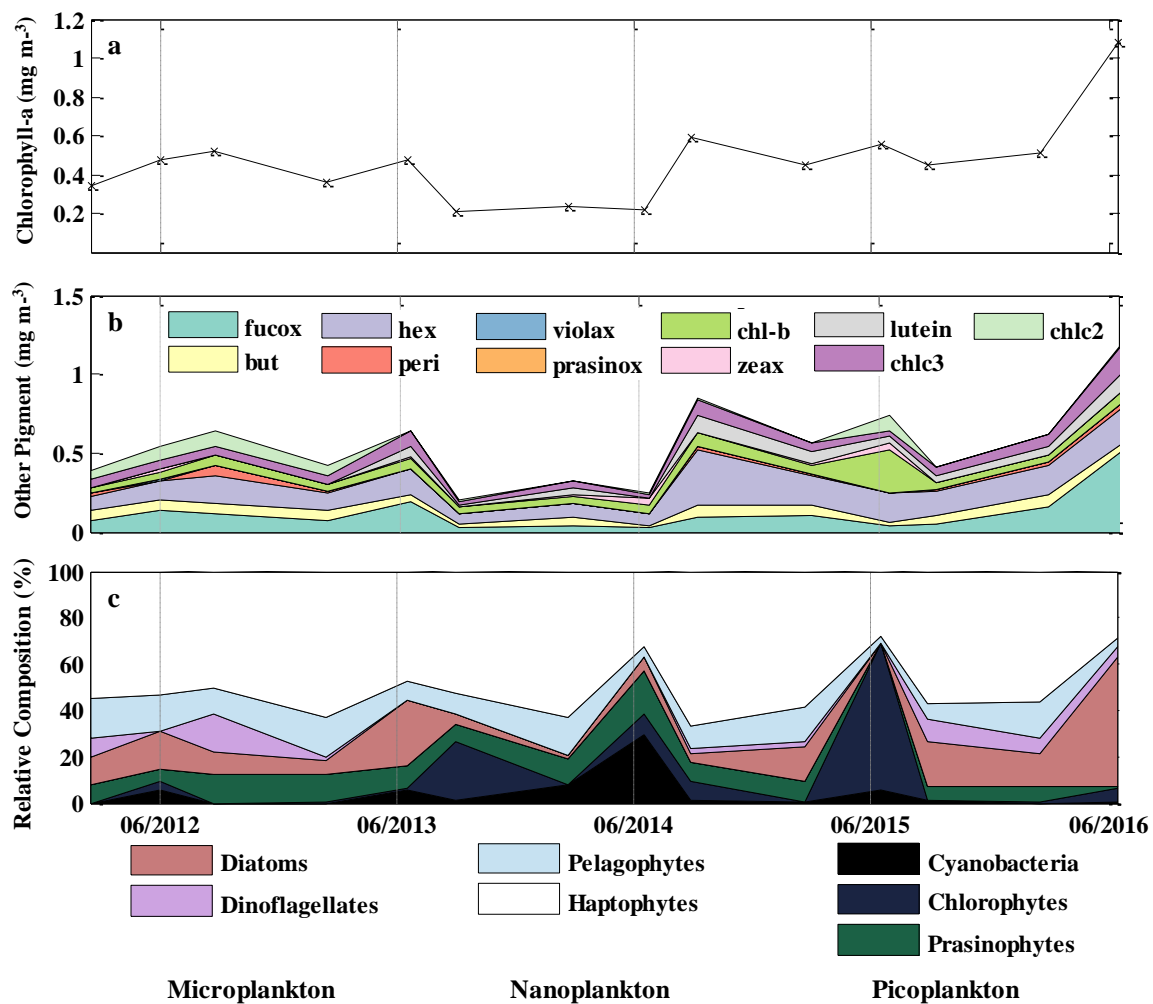
571  
572  
573  
574  
575  
576

**Figure 3** Schematic of the multi-layer upper ocean oxygen mass balance model (adapted from *Bushinsky and Emerson, 2015*). Fluxes ( $F$ ) are from air-sea gas exchange ( $F_{A-W}$ , including diffusion and bubble processes), vertical advection ( $F_V$ ), diapycnal eddy diffusion ( $F_{Kz}$ ), and entrainment ( $F_E$ ).





577  
 578 **Figure 4** (a-c) Upper ocean density, oxygen concentration, and oxygen supersaturation  $\Delta O_2$  (%)  
 579 from the SOS-Argo float at OSP. The thin black line indicates the mixed layer depth, the thick  
 580 blue line indicates the pycnocline depth, and the white rectangles indicate the modeled “upper  
 581 ocean” for each of the four years that ANCP were calculated. (d) Mixed layer DIC normalized to  
 582 a surface salinity at OSP ( $S=32.5$ ) from June 2012 to June 2016. Dash line boxes indicate  
 583 periods when the  $pCO_2$  data were not available and thus were filled with a straight line  
 584 interpolation.



585  
 586 **Figure 5** Mixed layer mean (a) chl-*a* concentration ( $\text{mg m}^{-3}$ ), (b) other pigment concentration  
 587 ( $\text{mg m}^{-3}$ ), and (c) relative phytoplankton composition (%) at OSP. Values were determined from  
 588 HPLC pigment analysis of samples collected in February, June, and August for each year from  
 589 2012 to 2016.

590

**Table 1.** Pigment:Chl *a* ratios for eight algal groups: (a) CHEMTAX initial ratio matrix, and (b) ranges of final pigment ratios obtained by CHEMTAX on the pigment data.

	Chl <i>c</i> <sub>3</sub>	Chl <i>c</i> <sub>2</sub>	Peri	But	Fuco	Pras	Viola	Hex	Allo	Zea	Lut	Chl <i>b</i>	Chl <i>a</i>
(a)													
Cyano	0	0	0	0	0	0	0	0	0	0.64	0	0	1
Chloro	0	0	0	0	0	0	0.049	0	0	0.032	0.17	0.32	1
Prasino	0	0	0	0	0	0.25	0.054	0	0	0.058	0.021	0.73	1
Crypto	0	0.2	0	0	0	0	0	0	0.38	0	0	0	1
Diatoms	0.08	0.28	0	0	0.99	0	0	0	0	0	0	0	1
Dinofla	0	0.22	0.56	0	0	0	0	0	0	0	0	0	1
Pelago	0.22	0	0	0.64	0.772	0	0	0	0	0	0	0	1
Hapto	0.18	0.21	0	0.039	0.289	0	0	0.47	0	0	0	0	1
(b)													
Cyano	0	0	0	0	0	0	0	0	0	0.48-0.85	0	0	1
Chloro	0	0	0	0	0	0	0.02-0.15	0	0	0.03-0.04	0.06-0.21	0.26-0.45	1
Prasin	0	0	0	0	0	0.04-0.23	0.02-0.06	0	0	0.02-0.06	0.017-0.022	0.72-1.12	1
Crypto	0	0.15-0.23	0	0	0	0	0	0	0.34-0.44	0	0	0	1
Diatoms	0.05-0.09	0.21-0.3	0	0	0.8-1.15	0	0	0	0	0	0	0	1
Dinofla	0	0.19-0.26	0.45-0.64	0	0	0	0	0	0	0	0	0	1
Pelago	0.11-0.25	0	0	0.68-1.15	0.22-0.82	0	0	0	0	0	0	0	1
Hapto	0.05-0.22	0.16-0.26	0	0.037-0.068	0.07-0.25	0	0	0.58-0.81	0	0	0	0	1

Abbreviations: Cyano, cyanobacteria; Chloro, chlorophytes; Prasino, prasinophytes; Crypto, cryptophytes; Dinofla, dinoflagellates; Pelago, pelagophytes; Hapto, haptophytes; Chl *c*<sub>3</sub>, chlorophyll *c*<sub>3</sub>; Chl *c*<sub>2</sub>, chlorophyll *c*<sub>2</sub>; Peri, peridinin; But, 19'-butanoyloxyfucoxanthin; Fuco, fucoxanthin; Pras, prasinoxanthin; Viola, violaxanthin; Hex, 19'-hexanoyloxyfucoxanthin; Allo, alloxanthin; Zea, zeaxanthin; Lut, lutein; Chl *b*, chlorophyll *b*; Chl *a*, chlorophyll.

**Table 2** Annual net community production (ANCP) determined from (a) O<sub>2</sub> mass balance, and (b) DIC mass balance. The annually integrated fluxes for each of the important terms (columns 4-9) indicate that the air sea flux and biological production terms dominate for both tracers. Two ANCP values are given in (a): one integrated from the ocean surface to the depth of annual mean pycnocline (column 3), ANCP, and another value integrated over the depth of the mixed layer, ANCP<sub>mixed layer</sub>. Only the former is a measure of the biological organic carbon that escapes the upper ocean on an annual basis (see text).

<b>a</b>										
Year	Time Period (June to June)	h (m)	Annual oxygen mass balance (mol O <sub>2</sub> m <sup>-2</sup> yr <sup>-1</sup> )						ANCP = J <sub>NCP</sub> /1.45 (mol C m <sup>-2</sup> yr <sup>-1</sup> )	ANCP <sub>mixed layer</sub> (mol C m <sup>-2</sup> yr <sup>-1</sup> )
			dh[O <sub>2</sub> ]/dt	F <sub>A-W</sub> = F <sub>s</sub> + F <sub>b</sub>	F <sub>E</sub>	F <sub>Kz</sub>	F <sub>V</sub>	J <sub>NCP</sub>		
1	2012-13	91	-0.7	-2.9	0	-0.6	-0.6	3.5	2.4 ± 0.6	3.4
2	2013-14	111	-1.3	-1.5	0	-0.8	-0.2	1.2	0.8 ± 0.4	1.3
3	2014-15	95	-0.6	-1.7	0	-0.9	-1.0	3.0	2.1 ± 0.4	2.3
4	2015-16	103	0.8	-0.1	0	-0.7	-0.3	2.3	1.6 ± 0.4	2.3

<b>b</b>										
Year	Time Period (June to June)	h (m)	Annual DIC mass balance (mol C m <sup>-2</sup> yr <sup>-1</sup> )						ANCP = - J <sub>NCP</sub> (mol C m <sup>-2</sup> yr <sup>-1</sup> )	
			dh[DIC]/dt	F <sub>A-W</sub>	F <sub>E</sub>	F <sub>Kz</sub>	F <sub>V</sub>	J <sub>NCP</sub>		
1	2012-13	91	-0.2	1.0	0	0.7	0.1	-2.0	2.0	
2	2013-14	111	-0.1	1.5	0	0.4	0.1	-2.1	2.1	
3	2014-15	95	0.05	2.0	0	0.5	0.1	-2.6	2.6	
4	2015-16	103	-0.04	2.0	0	0.9	0.1	-3.0	3.0	

**Table 3** ANCP calculated from O<sub>2</sub> mass balance with different start dates to determine if the chosen annual period affects the conclusions (see text).

Start Time		6/10/12	7/10/12	8/10/12
ANCP (mol C m <sup>-2</sup> yr <sup>-1</sup> )	1 <sup>st</sup> year (2012-13)	2.4	2.3	2.4
	2 <sup>nd</sup> year (2013-14)	0.8	0.9	0.7
	3 <sup>rd</sup> year (2014-15)	2.1	2.6	2.5
	4 <sup>th</sup> year (2015-16)	1.6	-	-

**Table 4** Comparisons of ANCP measured with O<sub>2</sub> mass balance and ANCP predicted from the temperature dependence parameterization of planktonic metabolism using parameters from the Arctic Ocean [*Regaudie-De-Gioux and Duarte, 2012*]. Gross primary production (GPP) is calculated from ANCP in year 1 and Equation 7, and it is assumed to be the same through years 1 – 4.  $ANCP_{diff} = 2.4 \text{ (mol C m}^{-2} \text{ yr}^{-1}) - ANCP_{\text{Predicted or Measured}}$

Year	Mean temperature (°C)	ANCP (mol C m <sup>-2</sup> yr <sup>-1</sup> )		ANCP <sub>diff</sub> (mol C m <sup>-2</sup> yr <sup>-1</sup> )	
		Predicted	Measured	Predicted	Measured
1	8.4	-	2.4	-	-
2	10.4	1.9	0.8	-0.5	-1.6
3	10.8	1.9	2.1	-0.5	-0.3
4	9.9	2.1	1.6	-0.3	-0.8